Electric Power Systems Research 123 (2015) 85–91

Contents lists available at ScienceDirect

Electric Power Systems Research

journal homepage: www.elsevier.com/locate/epsr

Real-time digital simulation-based modeling of a single-phase single-stage PV system

Javad Khazaei, Zhixin Miao, Lakshan Piyasinghe, Lingling Fan*

Department of Electrical Engineering, University of South Florida, Tampa, FL 33620, USA

ARTICLE INFO

Article history:
Received 2 December 2014
Received in revised form 29 January 2015
Accepted 30 January 2015

Keywords:
Incremental conductance (IC)
Real-time laboratory (RT-LAB)
Maximum power point tracking (MPPT)
Proportional resonant (PR) controller
Single-phase single-stage PV
Discrete models

ABSTRACT

This paper presents real-time digital simulation-based modeling of a single-phase single-stage PV system. Discrete models of voltage source converter (VSC) controls, including proportional resonant (PR) current control and phase-locked-loop (PLL) are developed in RT-LAB. An improved incremental conductance-based maximum power point tracking (MPPT) method that can mitigate error signal spikes is proposed and modeled in RT-LAB as well. Simulation results demonstrate the faster response of the proposed MPPT and the real-time simulation performance of the developed system model.

1. Introduction

Photovoltaic (PV) is considered as a widely spread source of renewable energy due to its low operational cost, low maintenance cost, and most importantly for being environment friendly without pollution. According to the literature, PV cells will become the most important alternative renewable energy sources till 2040 [1–5].

Real-time digital simulation based high-fidelity modeling can give a close-to-reality representation of the system dynamic performance. In addition, real-time simulation speed can be reached. Such simulation model can be used for prototype operation and control tests.

Modeling PV systems in real-time digital simulation has been mentioned in Ref. [6] where a PV serving a load through a dc/dc converter is modeled and simulated in RTDS. In another paper [7], a PV cell, its dc-link capacitor and a dc chopper are modeled in RT-LAB while the physical controller for the chopper is integrated into the software simulation model through RT-LAB interface. A grid-connected PV system has a more complicated control system. Modeling of such a system has not been seen in the literature. The objective of this paper is to model a single-phase single-stage PV system in RT-LAB.

Control of the interfacing dc/ac converter, including PR current control, PLL and MPPT will all be modeled in RT-LAB. In addition, an improved MPPT will be proposed and modeled in this paper. Various types of MPPT algorithms have been proposed in the recent years, *e.g.*, hill climbing (HC) [8,9], perturb and observe (PO) [10–13], and incremental conductance (IC) [14,15]. Among these types of algorithms, HC and PO are two commonly used approaches because of their simple control structures. The disadvantages related to these methods are: increased losses at steady state due to large perturbation around maximum power point; reduced dynamic performance the dynamic behavior when there is a sudden change in irradiance or at any other sudden dynamic event [16–18]; and large oscillations around the maximum point [19].

On the other hand, IC methods are based on the fact that the slope of the PV array power curve versus voltage is zero at the maximum power point (MPP). IC method has a lot of advantages compared with PO method. It can exactly determine when the MPP is reached. In a PO method, there are oscillations around the MPP. Accuracy of the IC method in tracking the maximum power or responding to the irradiance changes is more than that of a PO method [16,17]. Less ripples in output power are experienced during the operation compared with PO method [19]. And finally dynamic behavior of the IC based methods are faster when an operating point change is applied to the system [19].

Complexity of the IC method has limited the widespread implementation of this algorithm [17]. In the literature many researchers have focused on improving the dynamic response and steady state accuracy of the IC method [19–23]. In Ref. [19], it is demonstrated that the dynamic response of the IC method can be greatly improved if a proportional integral (PI) controller is used.

* Corresponding author. Tel.: +1 813 974 2031; fax: +1 813 974 5250.
E-mail address: linglingfan@usf.edu (L. Fan).

http://dx.doi.org/10.1016/j.epsr.2015.01.023
0378-7796/

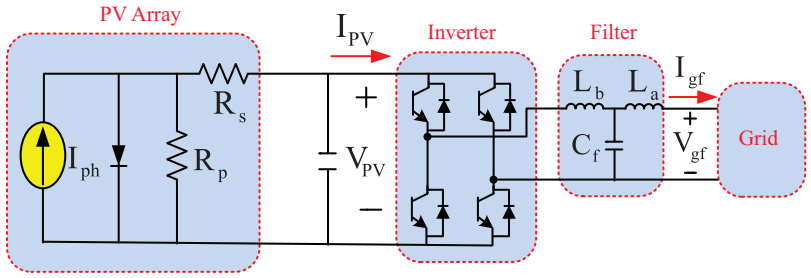

Fig. 1. Topology of a single-phase PV grid integration system. L_a = 10 mH, L_b = 20 mH, C_f = 10 μF, V_{gf} = 230 V. Sunpower PV panel: V_{PV} = 440 V, P_{PV} = 2.45 kW.

Moreover, if the output of the PI controller aims to modify the PV current instead of the PV inverter's duty cycle, the dynamic response is even better. A variable step-size IC MPPT is proposed in [24]. The step size is automatically adjusted according to the derivative of power to voltage () of a PV array. The step size will become tiny as becomes very small around the MPP. Thus, it provides a very good accuracy at steady state and the dynamics of the MPPT will be improved. However, the proposed method has added more complexity to the IC algorithm.

In this paper, a new algorithm is proposed which can improve the steady-state response and dynamic behavior of MPPT. In the proposed method, instead of using the traditional incremental error $\left(\frac{dI}{dV}+\frac{I}{V}\right)$ which could lead to spikes when dV is approaching zero, the proposed error will no longer contain dV at the denominator. This approach will remove the conditional statements from the IC-PI MPPT and lead to improvement in dynamic performance of the MPPT algorithm. The designed algorithm provides no oscillations around MPP (which was one of the main drawbacks of MPPT algorithms), and it can reach to the MPP very fast. Moreover, as the proposed algorithm is simple, it is easy to be implemented in real-time MPPT controller. Better efficiency, less calculation time and memory allocation compared to traditional algorithms can be achieved.

The rest of the paper is organized as follows: the system configuration will be described in Section 2. PV control models in RT-LAB, which consist of a PR controller and MPPT, are described in Section 3. Case studies are presented in Section 4. Section 5 presents the conclusion.

2. System configuration

The PV system configuration is illustrated in Fig. 1. The model is composed of a PV array, a dc/ac inverter, and a filter. The PV array is composed of a number of parallel connected PV strings. These PV strings consist of a number of serially connected PV cells. Parameters of these cells will be different for different commercial PV models. Each cell in a module can be modeled as a photo-generated current source in parallel with a diode and a shunt resistor, R_p, as well as in series with a series resistor, R_s as shown in Fig. 1.

I_{ph} is photo-generated current and is proportional to the irradiance which will be normalized by the short circuit current (I_{sc}) [25]:

$$I_{ph} = A_{ph} \cdot I_{sc} \cdot E_e \tag{1}$$

where E_e is the effective sun radiance considering the effect of incidence angles, transmission through glass, encapsulant and spectral responses of the cell. A_{ph} is the proportionality factor which is related to the cell temperature and is usually close to one. Current through the diode can be represented by the Shockley equation in the following [25]:

$$I_{diode} = I_{sat}\, e^{\frac{V_{PV}+I_{PV}\cdot R_s}{mV_T}} \tag{2}$$

where I_{sat} is the diode saturation current which strongly depends on the cell temperature. Cell voltage and current are notated as V_{PV} and I_{PV} respectively. m is the diode factor, a measure of ideality of the diode, usually a number between 1 and 2. In situations where the PV array is modeled by two parallel diodes, m is set to 1, the ideal factor.

V_T is the thermal voltage which is related to Boltzmann's constant k, the elementary charge q, and the cell temperature T_{cell} as shown in Ref. [25].

$$V_T = \frac{k \cdot T_{cell}}{q}. \tag{3}$$

3. PV control

The main block diagram of the PV control is illustrated in Fig. 2. The inputs of the MPPT block are the measurements from the PV array (I_{PV}, V_{PV}). The output of the MPPT block is then modified to shape the reference PV AC current magnitude. The measured AC current of the grid is then compared with the reference signal and the error will be sent to the proportional resonance (PR) controller. The output of the PR controller is then sent to the PWM block to generate the pulses for the PV inverter. A single-phase phase-locked-loop (PLL) is used to synchronize the PV reference current with the AC grid in Fig. 2.

Since the real-time simulators are working in discrete time domain, all the controllers are modeled in discrete time domain. Detailed parameters of the PLL, the MPPT, and the PR controller are given in Table 1.

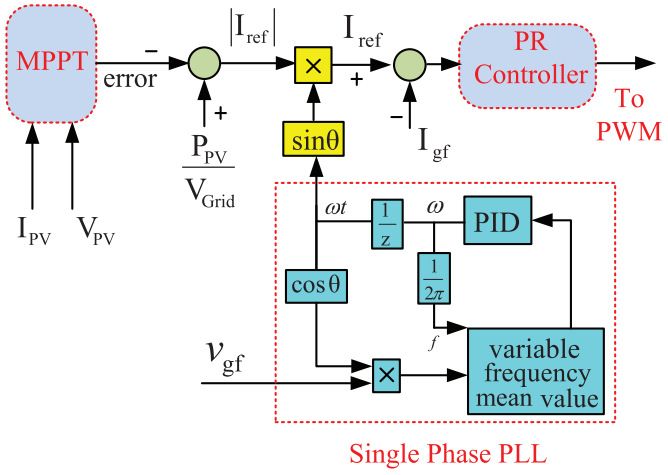

Fig. 2. Block diagram of PV control system.

Table 1
Parameters of single phase PV for Sunpower Panel.

Total capacity	2.4 kW
Nominal voltage	440 V
Open circuit voltage per cell	64.2 V
Short circuit current per cell	5.96 A
K_p, K_r of PR controller	100, 500
ω	377 rad/s
K_p, K_i of MPPT controller	5, 20
K_p, K_i of PLL	180, 3200
L_b, L_a of AC filter	20, 10 mH
C of AC filter	1 μF
Frequency	60 Hz

3.1. Discrete time single phase PLL

The main task of phased-locked-loop (PLL) is to provide a reference phase signal synchronized with the AC systems. The reference phase is then used to generate a carrier waveform for firing pulses in control circuits of converters. PLL has the capability to dynamically change the reference phase due to any dynamic change in AC systems, ensuring synchronization of the converter's output with the AC system.

The PLL model in Simpower systems was developed by Pierre Giroux in 2007. Description of the PLL models can also be found in [26]. The continuous time PLL model will be converted to a model in discrete time. The main block diagram of the discrete time PLL is illustrated in Fig. 3, derived based on Fig. 2.

The input of the PLL is the grid AC voltage, v_{gf}, and the output is the frequency or angle which is synchronized with the grid. Furthermore, there is a variable frequency mean value calculator represented by a simple integrator and a delay block. Suppose v_{gf} is sinusoidal and can be expressed as $v_{gf} = V_{gf} \sin\theta_g$. Then multiplied by $\cos\theta$, we have

$$V_q = \frac{1}{2} V_{gf}(\sin(\theta_{gf} + \theta) + \sin(\theta_{gf} - \theta)). \tag{4}$$

There are two components in V_q, one is of high frequency and the other will be a low frequency one. If the angular speeds of θ_{gf} and θ match each other, then the second component is a dc value. After passing the integrator, the effect will be mainly due to the second component as the integration of the high-frequency component will be around zero. The objective of the PI controller will bring the second component in V_q to zero, i.e., $\theta_{gf} = \theta$. Thus, PLL can obtain the angle of v_{gf}. The frequency of the grid voltage can also be obtained.

3.2. Discrete proportional resonant (PR) controller

A PR controller provides an infinite gain in a very narrow bandwidth that is centered at the resonance frequency (ω). As a result, steady-state error is eliminated at the resonance frequency ω. Therefore, a PR controller can track a sinusoidal reference signal. For a single-phase PV converter, the error signal is the mismatch of the grid AC reference current and measured grid instantaneous current. The general control block of the PR controller is illustrated in Fig. 4.

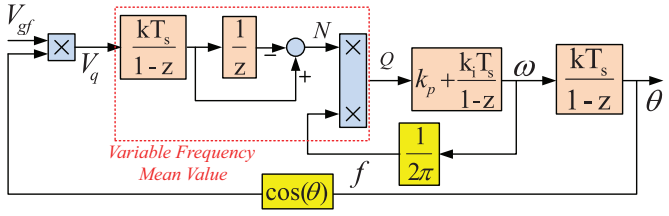

Fig. 3. Discrete-time model of a single-phase PLL for the PV system.

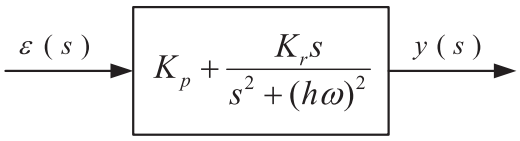

Fig. 4. Control diagram of PR controller.

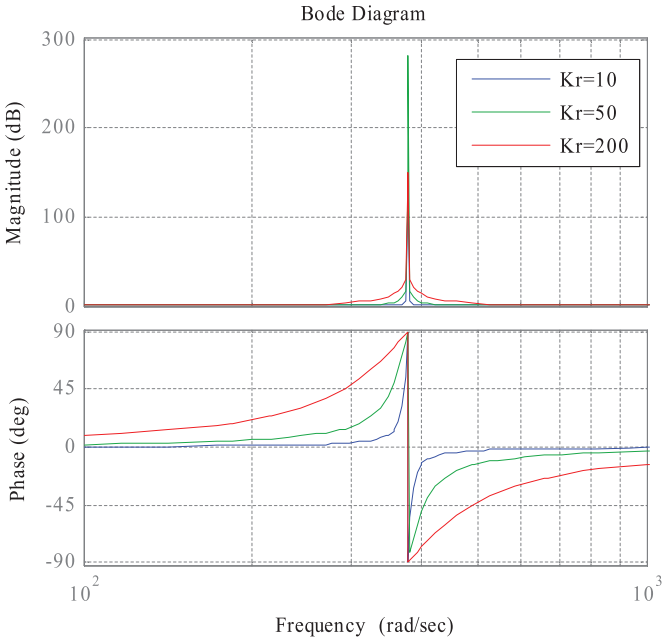

Fig. 5. Bode plot for PR controller for different K_r while $K_p = 1$ and $\omega = 377$ rad/s.

The Bode plots of a PR controller with different resonance gains are illustrated in Fig. 5. It can be observed that at frequencies close to 377 rad/s or 60 Hz, the PR controller's gain is very large. This in turn will cause the gain of the close-loop system very small at this frequency. Therefore, steady-state error at ω will approach zero. In this study, the PR controller for the single-phase PV has been designed to compensate the high order frequencies of: 3rd, 5th, 7th, and 9th.

The PR controller will be modeled in discrete time for RT-LAB. The original system can be expressed as follows.

$$y(s) = \underbrace{K_p \varepsilon(s)}_{y_1(s)} + \underbrace{K_r \frac{s}{s^2 + \omega^2} \varepsilon(s)}_{y_2(s)} \tag{5}$$

The proportional block will be kept the same in the discrete domain. In contrast, converting $y_2(s)$ into discrete form requires derivation. The procedure can be found in Ref. [27] and also described as follows. Rearranging $y_2(s)$ will leads to:

$$\begin{aligned} y_2(s) &= K_r \frac{s}{s^2 + \omega^2} \varepsilon(s) \\ \frac{s^2 + \omega^2}{s^2} y_2(s) &= \frac{K_r}{s} \varepsilon(s) \\ y_2(s) + \frac{\omega^2}{s^2} y_2(s) &= \frac{K_r}{s} \varepsilon(s) \\ y_2(s) &= \frac{1}{s} \left[K_r \varepsilon(s) - \frac{1}{s} \omega^2 y_2(s) \right]. \end{aligned} \tag{6}$$

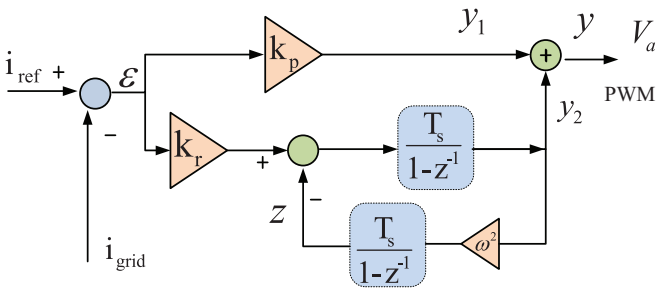

Fig. 6. Structure of PR controller.

Defining a new variable z, the simplified model of $y_2(s)$ is expressed by:

$$\begin{cases} y_2(s) &= \frac{1}{s}\left[K_r\varepsilon(s) - z(s)\right] \\ z(s) &= \frac{1}{s}\omega^2 y_2(s). \end{cases} \tag{7}$$

Discretizing (7) is now limited to an integrator which should be changed from s-domain into discrete time integrator, where $1/s$ corresponds to $\frac{T_s}{1-z^{-1}}$. The block diagram of the proposed controller has been illustrated in Fig. 6, but due to the space limitations, only the first harmonic has been shown here.

The PR controller aims to control the grid side AC current. To achieve this objective, the error of the reference PV current and measured PV current will be used as the input for the PR controller. The reference current magnitude generated from the output of the MPPT block will be synchronized with the grid voltage before sending to the PR controller. The synchronization steps will be carried out in a single-phase PLL block. The output of the PR controller is the voltage reference which will be directly sent to the pulse width modulation (PWM) generation unit.

3.3. MPPT for PV systems

The MPPT is the main part in the photovoltaic systems which can ensure the maximum captured power from the PV array. It continuously tunes the system regardless of weather or load condition change such as: irradiance change, ambient temperature, or wind which can affect the PV array output. Conventional MPPT algorithms use $dP/dV = 0$ to ensure the maximum power harvest.

3.3.1. Traditional IC method

The incremental conductance technique has been implemented here which directly focuses on power variations. It means the power slope of the PV is zero at MPP $\left(\frac{dP}{dV} = 0\right)$, positive in the left hand side of MPP and negative in the right hand side. The output current and voltage of the PV panel are used to calculate the conductance and incremental conductance. The basic approach is to compare the conductance (I/V) with the incremental conductance (dI/dV) and decide when to increase or decrease the PV voltage. In order to reach the maximum power point, the derivative of the power (dP/dV) should be always zero. Considering $P = V \cdot I$ [17]:

$$\frac{dP}{dV} = \frac{d(V \cdot I)}{dV} = I + V\frac{dI}{dV} = 0 \tag{8}$$

$$\Rightarrow \frac{dI}{dV} = -\frac{I}{V} \tag{9}$$

which means when the conductance is opposite of the incremental conductance, the maximum power is guaranteed.

The discrete real-time traditional IC MPPT model is shown in Fig. 7. The conductance will be added to the incremental conductance to generate an error signal. The objective of the PI controller

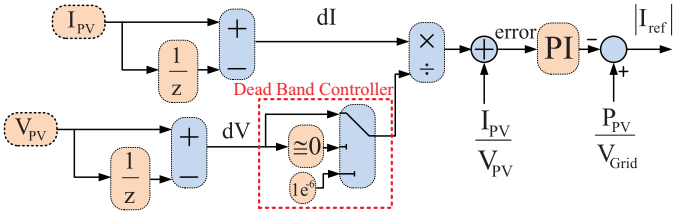

Fig. 7. The MPPT structure for a single-phase PV in RT-LAB.

is to make the error signal approach zero. For real-time simulations of IC, the output of the MPPT is directly sent to the current controller loop to take the advantage of the fast response of the current controller loop. Here the output of the MPPT block will be added to a constant (PV power divided by the grid voltage RMS) to form the magnitude of reference current value. This current reference will be used in the current control to adjust the grid current by means of a PR controller. A dead band is used to at $dV = 0$ conditions. If dV becomes zero, the error will be infinity and the proposed MPPT algorithm will not work properly. The traditional dead-band controller in Fig. 7 shows that if dV is zero, a very small value is considered $(1e^{-6})$ to avoid the error to be infinity. The problem with traditional dead-band controller is that even the value of dV is set to a small value, large spikes in the output of MPPT will appear when dV is oscillating around zero. This is not acceptable for the controller.

MPPT mechanism Fig. 8 shows the sample V–I characteristic of a PV. Suppose the operating point is at Point 1 where the error is greater than zero. According to the MPPT in Fig. 7, the output of the PI unit will increase, which in turn leads to the decrease in the AC current reference. The grid voltage is constant. In addition, the current control response is much faster than MPPT and the current is synchronized with the grid voltage through PLL. Therefore, this leads to the reduction in active power at the AC side. Ignore the loss of the switches, the average power at the dc side should be the same of that at the ac side. Therefore, at the dc side of the converter, if we assume that the dc voltage V_{PV} is kept the same, then the dc current I_{PV} will have a reduction due to the reduction in the AC current magnitude. Reduction in I_{PV} will leads to increase in V_{PV} and P_{PV}. Until the error reaches zero, the PI control will keep adjusting the AC current reference.

Similarly, when the PV system is at Point 3 where the error is less than zero, then the AC current reference will have an increase, which in turn leads to the increase in I_{PV} and the reduction in V_{PV}. The combination leads to the increase in P_{PV}. It is possible to have *oscillations* in power if the gains of the PI controller are large. This can lead to too much increase in the AC current reference and I_{PV}. At that point, the error signal becomes greater than zero. The AC

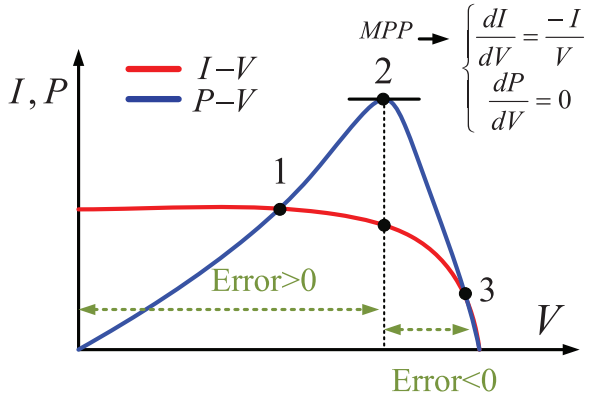

Fig. 8. Error signal description based on I–V characteristic of PV.

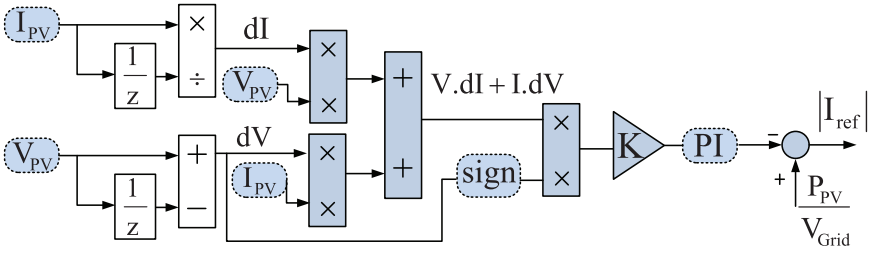

Fig. 9. Improved IC MPPT for PV systems.

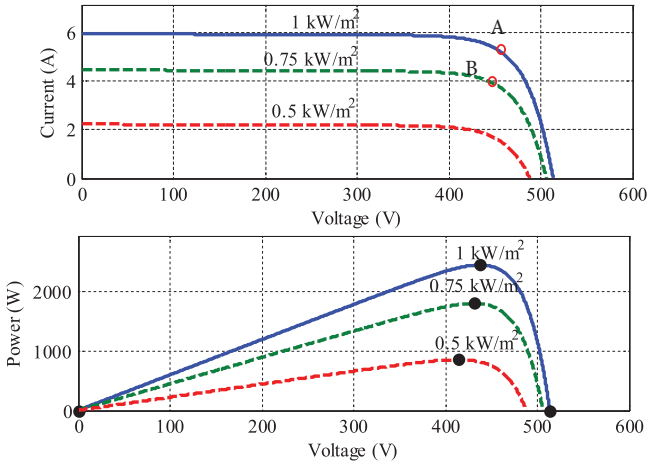

Fig. 10. *V–I* and *P–V* curves for different irradiance values of Sunpower PV panel.

current reference then will see a reduction, so on and so forth till the error approaches zero.

3.3.2. Modified IC-PI MPPT

For traditional IC-PI MPPT, when dV reaches to zero, the error signal will go to infinity and the output of the MPPT will have a spike. To solve e problem, the proposed algorithm suggests that the dV should be removed from the denominator of the error signal. Modified error signal can be considered as: $V \cdot dI + I \cdot dV$, which can be viewed as the previous error signal $\left(\frac{dI}{dV} + \frac{I}{V}\right)$ multiplied by $V \cdot dV$.

In this case, dV is no longer in the denominator and it will not cause any spikes in MPPT output even when dV is zero. However, the

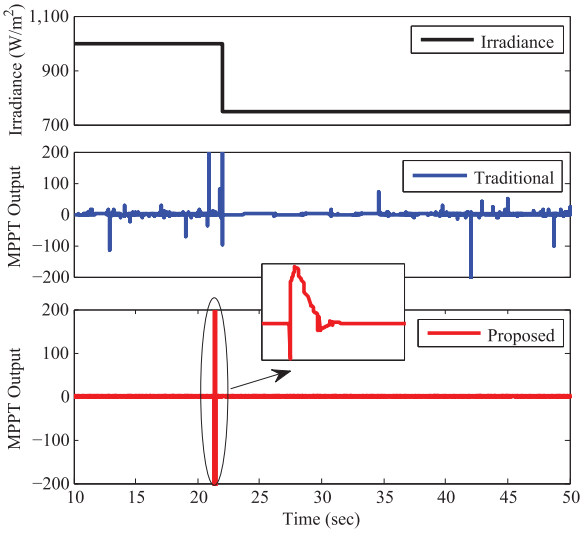

Fig. 11. Irradiance step change and the MPPT input error.

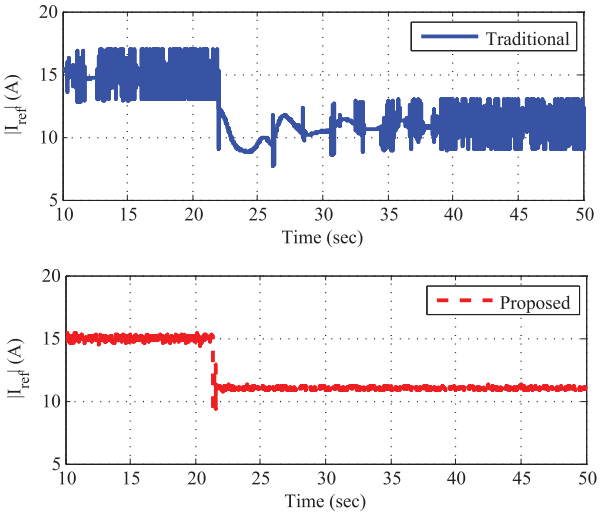

Fig. 12. The AC current magnitude reference.

error signal should provide the same implication of operation point position as the previous error signal. Modification is presented as follows.

Analysis of the error signal used in traditional IC is presented as follows.

$$\text{If } error > 0 \left(\frac{dI}{dV} > -\frac{I}{V}\right) \Rightarrow \begin{cases} dV > 0 \Rightarrow VdI + IdV > 0 \\ dV < 0 \Rightarrow VdI + -IdV < 0 \end{cases} \quad (10)$$

Eq. (10) shows that if the traditional error is positive, the sign of the proposed new error will depend on the sign of dV. If dV is positive, the defined new error will be positive, same as the traditional error; but if dV is negative, the proposed new error will be

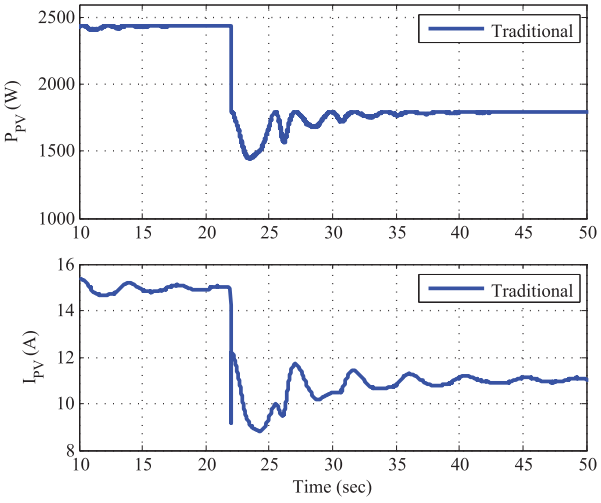

Fig. 13. PV output power and dc current for traditional MPPT.

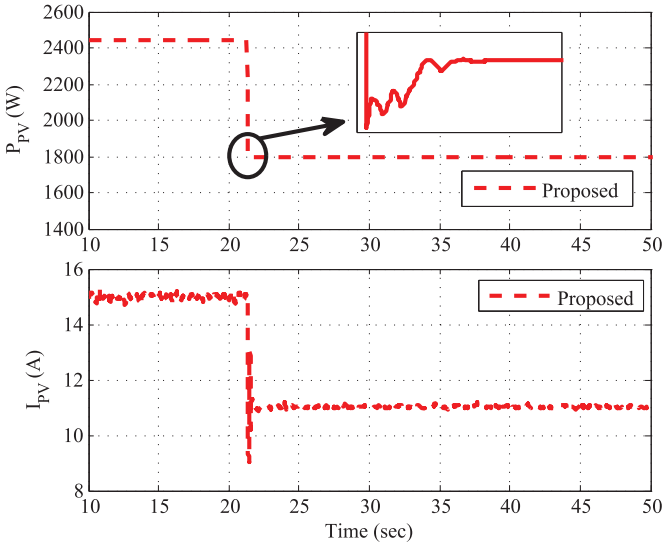

Fig. 14. PV output power and dc current for the proposed MPPT.

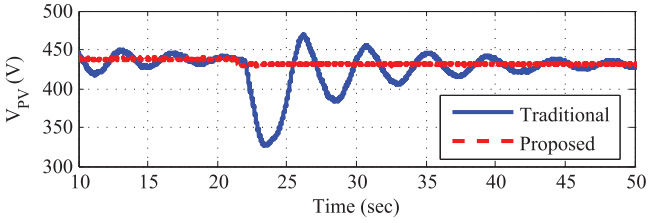

Fig. 15. PV voltage.

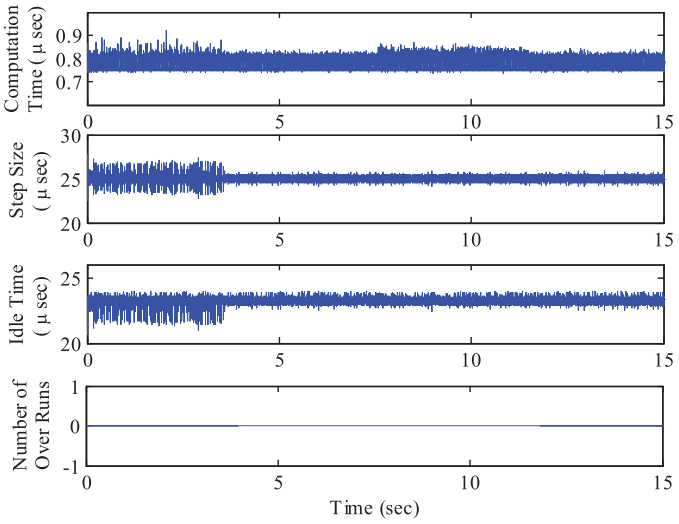

Fig. 16. Simulation results from Opmonitor Block.

negative, which is a contradiction. Same thing happens when the error is negative:

$$\text{If error} < 0 \quad \left(\frac{dI}{dV} < -\frac{I}{V}\right) \Rightarrow \begin{cases} dV > 0 \Rightarrow VdI + IdV < 0 \\ dV < 0 \Rightarrow VdI + IdV > 0 \end{cases} \tag{11}$$

Therefore, a modification can be proposed to ensure the modified error signal having the same implication of operation point as the traditional error signal.

The new error is now multiplied by the sign of dV. The sign of the new error will always agree with the sign of the traditional error. The proposed error is very small compared with traditional error signal, which justifies a large gain ($K = 1000$) before applying this error to a discrete PI controller. The improved MPPT algorithm is illustrated in Fig. 9. As it can be seen, the error signal will be magnified by a gain, then the output will be sent to the PI controller.

4. Case studies

This section is dedicated to real-time simulation results which have been conducted in real-time digital simulator RT-LAB. A real PV model named as Sunpower SPR 305 WHT is considered for verification of the proposed algorithm for IC-PI MPPT method. The PV model is composed of 96 cells combined in 8 series PV strings. For this type of PV panels, I_{ph} equals to 5.96 A, $R_p = 900\,\Omega$ and $R_s = 0.038\,\Omega$. The V–I and P–V curves for different irradiance values have been illustrated in Fig. 10.

Different irradiance values will provide different V–I curves. For 1 kW/m^2, the maximum power will be around 2.45 kW when the voltage is 440 V. For the dynamic event, a step change to the irradiance is applied by decreasing the irradiance at $t = 21$ s from 1 kW/m^2 to 0.75 kW/m^2. Such a step change is illustrated in Fig. 11.

The input error for MPPT controller for both algorithms has also been shown in Fig. 11. It shows that the traditional method is suffering from a lot of spikes during the simulation because the error is oscillating around zero which makes the dead-band controller to act. In contrast, the proposed algorithm provides no spikes.

The AC current magnitude reference $|I_{ref}|$ is plotted in Fig. 12 for both traditional MPPT and proposed MPPT. It can be observed that the proposed MPPT results in a much smoother $|I_{ref}|$.

Simulation results of the PV output power and current following the applied irradiance change are illustrated in Figs. 13 and 14. As it can be observed, after the sudden irradiance change, the traditional IC-PI method will face a lot of dynamics and it takes a long time for the active power to be settled to its new reference value. In contrast, the proposed IC method can respond to the sudden dynamic event very fast and it will be settled to the new reference value shortly.

The dc voltage is shown in Fig. 15. As the irradiance is changed at 21 s, the maximum power is then set to the new value and referring to the V–I characteristic presented in Fig. 10, the output voltage will be set to the new value (425 V), which is less than the previous value. Compared with the traditional method, the proposed method can fix the voltage to the new set-point very fast and without much dynamics.

Results of operating point change have shown a great improvement in the MPPT algorithm. The proposed algorithm is not only easy to be implemented but also provides a faster response and improved dynamic performance of the PV energy systems.

4.1. RT-LAB performance

To examine the performance of real-time simulators, the performance metrics of the model are extracted through Opmonitor Block in the RT-LAB. Opmonitor block provides necessary information regarding the performance or RT-LAB. It mainly records computation time, step size, idle time, and number of overruns. Computation time is the time spent in calculation of the previous step time excluding the communication overhead in μs. Step size clarifies the real step size which has been selected for the model during the run which is 25 μs in this study. Idle time is the idle time during the execution of previous time step. Idle time plus computation time should be equal to the real step size. Number of overruns is the number of overruns during the run which is zero in this case clarifying the stable condition of running. The results of the Opmonitor Block are included in Fig. 16. In this case study, the computation time is less than 1 microsecond which clarifies the CPU usage of the model less than 4% $\left(\frac{25-24}{25} \times 100\%\right)$, which is a great performance.

Furthermore, there is no overrun detected by the simulator which means all the cores are performing in a balanced manner.

5. Conclusion

This paper presents real-time digital simulation-based modeling of a single-phase single-stage PV grid integration system. Models for the PV panel, PLL, PR current control and MPPT are all developed in discrete domain. In addition, an improved MPPT algorithm is proposed this paper. The proposed MPPT algorithm does not need dead-band blocks used in traditional IC MPPT control. Simulation case studies demonstrate that the proposed MPPT has a superior performance than the traditional MPPT.

Acknowledgements

This research is supported in part by Duke Energy through Community Power System Simulation project. The authors acknowledge OPAL-RT for support in RT-LAB setup.

References

[1] B. Liu, S. Duan, T. Cai, Photovoltaic dc-building-module-based BIPV system-concept and design considerations, IEEE Trans. IEEE Power Electron. 26 (5) (2011) 1418–1429.
[2] B. Yang, W. Li, Y. Zhao, X. He, Design and analysis of a grid-connected photovoltaic power system, IEEE Trans. IEEE Power Electron. 25 (4) (2010) 992–1000.
[3] Y.-H. Ji, D.-Y. Jung, J.-G. Kim, J.-H. Kim, T.-W. Lee, C.-Y. Won, A real maximum power point tracking method for mismatching compensation in PV array under partially shaded conditions, IEEE Trans. IEEE Power Electron. 26 (4) (2011) 1001–1009.
[4] L. Zhang, K. Sun, Y. Xing, L. Feng, H. Ge, A modular grid-connected photovoltaic generation system based on dc bus, IEEE Trans. IEEE Power Electron. 26 (2) (2011) 523–531.
[5] J.L. Agorreta, M. Borrega, J. López, L. Marroyo, Modeling and control of-paralleled grid-connected inverters with LCL filter coupled due to grid impedance in pv plants, IEEE Trans. IEEE Power Electron. 26 (3) (2011) 770–785.
[6] M. Park, I.-K. Yu, A novel real-time simulation technique of photovoltaic generation systems using RTDS, IEEE Trans. Energy Convers. 19 (March (1)) (2004) 164–169.
[7] O. Crăciun, A. Florescu, S. Bacha, I. Munteanu, A. Bratcu, Hardware-in-the-loop testing of PV control systems using RT-LAB simulator, in: 2010 14th International Power Electronics and Motion Control Conference (EPE/PEMC), September, 2010, S2-1–S2-6.
[8] S.B. Kjaer, Evaluation of the "hill climbing" and the "incremental conductance" maximum power point trackers for photovoltaic power systems, IEEE Trans. Energy Convers. 27 (4) (2012) 922–929.
[9] W. Xiao, W.G. Dunford, A modified adaptive hill climbing MPPT method for photovoltaic power systems, in: 2004 IEEE 35th Annual Power Electronics Specialists Conference, PESC 2004, vol. 3, IEEE, 2004, pp. 1957–1963.
[10] A.K. Abdelsalam, A.M. Massoud, S. Ahmed, P. Enjeti, High-performance adaptive perturb and observe MPPT technique for photovoltaic-based microgrids, IEEE Trans. Power Electron. 26 (4) (2011) 1010–1021.
[11] M.A. Elgendy, B. Zahawi, D.J. Atkinson, Assessment of perturb and observe MPPT algorithm implementation techniques for PV pumping applications, IEEE Trans. Sustain. Energy 3 (1) (2012) 21–33.
[12] D. Sera, R. Teodorescu, J. Hantschel, M. Knoll, Optimized maximum power point tracker for fast changing environmental conditions, in: 2008 IEEE International Symposium on Industrial Electronics, ISIE 2008, IEEE, 2008, pp. 2401–2407.
[13] G. Petrone, G. Spagnuolo, R. Teodorescu, M. Veerachary, M. Vitelli, Reliability issues in photovoltaic power processing systems, IEEE Trans. Ind. Electron. 55 (7) (2008) 2569–2580.
[14] A. Safari, S. Mekhilef, Simulation and hardware implementation of incremental conductance MPPT with direct control method using cuk converter, IEEE Trans. Ind. Electron. 58 (4) (2011) 1154–1161.
[15] A. Safari, s. Mekhilef, Incremental conductance MPPT method for PV systems, in: 24th IEEE Canadian Conference on Electrical and Computer Engineering (CCECE 2011), IEEE, 2011, pp. 345–347.
[16] A. Pandey, N. Dasgupta, A.K. Mukerjee, Design issues in implementing MPPT for improved tracking and dynamic performance, in: IECON 2006 – 32nd Annual Conference of IEEE Industrial Electronics, IEEE, 2006, pp. 4387–4391.
[17] M. Ciobotaru, R. Teodorescu, F. Blaabjerg, Control of single-stage single-phase PV inverter, in: 2005 European Conference on Power Electronics and Applications, IEEE, 2005, p. 10.
[18] E. Koutroulis, F. Blaabjerg, A new technique for tracking the global maximum power point of PV arrays operating under partial-shading conditions, IEEE J. Photovolt. 2 (2) (2012) 184–190.
[19] M.A.G. de Brito, L. Galotto, L.P. Sampaio, G. de Azevedo e Melo, C.A. Canesin, Evaluation of the main mppt techniques for photovoltaic applications, IEEE Trans. Ind. Electron. 60 (3) (2013) 1156–1167.
[20] B. Liu, F. Duan, F. Liu, P. Xu, Analysis and improvement of maximum power point tracking algorithm based on incremental conductance method for photovoltaic array, in: 7th International Conference on Power Electronics and Drive Systems, IEEE, 2007, pp. 637–641.
[21] Q. Mei, M. Shan, L. Liu, J.M. Guerrero, A novel improved variable step-size incremental-resistance MPPT method for PV systems, IEEE Trans. Ind. Electron. 58 (6) (2011) 2427–2434.
[22] Z. Yan, L. Fei, Y. Jinjun, D. Shanxu, Study on realizing MPPT by improved incremental conductance method with variable step-size, in: 3rd IEEE Conference on Industrial Electronics and Applications, ICIEA 2008, IEEE, 2008, pp. 547–550.
[23] J.H. Lee, H. Bae, B.H. Cho, Advanced incremental conductance MPPT algorithm with a variable step size, in: 12th International Conference on Power Electronics and Motion Control, EPE-PEMC 2006, IEEE, 2006, pp. 603–607.
[24] F. Liu, S. Duan, F. Liu, B. Liu, Y. Kang, A variable step size INC MPPT method for PV systems, IEEE Trans. Ind. Electron. 55 (7) (2008) 2622–2628.
[25] S.R. Wenham, Applied Photovoltaics, Routledge, 2011.
[26] H. Pereira, A. Cupertino, C.A. da, S.G. Ribeiro, S. Silva, Influence of PLL in wind parks harmonic emissions, in: IEEE PES Innovative Smart Grid Technologies Conference – Latin America (ISGT LA), IEEE, 2013, pp. 1–8.
[27] R. Teodorescu, F. Blaabjerg, U. Borup, M. Liserre, A new control structure for grid-connected LCL PV inverters with zero steady-state error and selective harmonic compensation, in: Nineteenth Annual IEEE Applied Power Electronics Conference and Exposition, APEC'04, vol. 1, IEEE, 2004, pp. 580–586.